REFERENCES AND NOTES

1. R. Y. Koyanagi *et al.*, *Volcanism in Hawaii* (Government Printing Office, Washington, DC, 1987), pp. 1221–1257.
2. K. Kamo and K. Ishihara, *Bull. Disaster Prev. Res. Inst.* **29B**, 1 (1986); A. T. Linde *et al.*, *Nature* **365**, 737 (1993).
3. So-called single-force models have been applied to explain long-period seismic wave forms attributable to such mass advection at different volcanoes of the world [H. Kanamori and J. W. Given, *J. Geophys. Res.* **87**, 5422 (1982); K. Uhira and M. Takeo, *ibid.* **99**, 17775 (1994)]. Recent advances in seismometry have now made such observations rather straightforward; portable equipment covering a wide frequency band (50 to 0.01 Hz) can be easily installed at volcanoes, and the broadband nature of volcanic activity is becoming increasingly clear [H. Kawakatsu *et al.*, *Geophys. Res. Lett.* **19**, 1959 (1992); T. Ohminato *et al.*, *Eos* **74**, 648 (1993); R. Dreier *et al.*, *Acta Vulcanol.* **5**, 165 (1994); S. Falsaperla *et al.*, *ibid.*, p. 173; J. Neuberg *et al.*, *Geophys Res. Lett.* **21**, 749 (1994); P. Hellweg *et al.*, *Eos* **75**, 313 (1994)].
4. Seismic signals were recorded continuously with portable data loggers either on digital tapes, hard disks, or magneto-optical disks, with a sampling rate of 20 Hz and dynamic range of either 16 or 24 bits. Recorder clocks were either locked with GPS (Global Positioning System) or adjusted by radio time signals, providing accurate enough timing for later analyses of long-period signals.
5. Disturbances commonly called long-period events at volcanoes are in the period range 0.2 to 2 s [B. J. Chouet, *Nature* **380**, 309 (1996)].
6. Long-period seismometers installed at the Aso volcano 60 years ago revealed the presence of long-period (3.5 to 7 s) volcanic tremors [K. Sassa, *Mem. Coll. Sci. Kyoto Univ. Ser. A* **18**, 255 (1935)]. The observation of long-period volcanic tremors has been repeatedly reported [M. Churei, *Bull. Volcanol. Soc. Jpn.* **30**, 71 (1985); T. Hashida, *ibid.* **35**, 323 (1990); H. Kawakatsu *et al.*, *Geophys. Res. Lett.* **21**, 1963 (1994)], but those observations have fallen short of unraveling their origin because of the limited number of instruments near the crater.
7. One of the possible mechanisms generating the LPT may be resonance of a vertical crack filled with fluid [B. J. Chouet, *J. Geophys. Res.* **91**, 13967 (1986); V. Ferrazzini and K. Aki, *ibid.* **92**, 9215 (1987)]. The presence of waves trapped in the crack that propagate with a phase velocity much slower than the sound velocity of the fluid—the so called "crack wave"—has been proposed. Consideration of the crack wave would greatly reduce the estimate of the size of the resonator.
8. N. Neidel and M. T. Tarner, *Geophysics* **36**, 483 (1971). To improve the resolution of source depth, we extended conventional single-component semblance analyses to three-component wave forms [H. Matsubayashi, thesis, Tokyo University (1995)].
9. Moment tensor inversion of LPT wave forms gives a best point source solution corresponding to a combination of isotropic expansion (contraction) and inflation (deflation) of a vertical crack aligned from north-northwest to south-southeast, parallel or subparallel to the chain of older craters (Fig. 1). A LPT source with a finite extent can be approximated by a summation of point sources. As long as we retain the above moment tensor solution throughout the source, LPT amplitudes at the stations located northeast or southwest of the crater (KHE and AWS) are greatly increased by putting point sources near these stations, and particle motions at these stations become too steep to match the observations, which may indicate that the effective extent of the LPT source does not exceed several hundred meters from the center of the crater.
10. S. Kikuchi, *Bull. Disaster Prev. Res. Inst.* **17B**, 1 (1974).
11. The meteorological station at Aso reported that the ash and smoke went up as high as 1 km when one of the eruptions took place at 06:31 (GMT) on 15 September. Shock waves were not reported for any of the eruptions. At the largest eruptions, ejecta of fragmented rocks ascended to a height of nearly 150 m above the crater lake, with corresponding initial velocities of the order of 50 m/s. The velocities of the steam that entrained those solid ejecta is bounded by the sound velocity in the atmosphere (330 m/s) and that of solid ejecta.
12. The presence of many different kinds of short-period tremors are known at Aso volcano (*6*), and here we specifically call the kind associated with phreatic eruptions SPT. Note also that the short-period tremors that we call SPTs here may be referred to as long-period events or tremors at other volcanoes (*5*).
13. G. S. Steinberg and A. S. Seinberg, *J. Geophys. Res.* **80**, 1600 (1975).
14. Larger eruptions tend to excite larger pressure waves at the time of mass ejection, which is recorded at a microbarograph near the crater (Fig. 1), although the correlation is rather weak.
15. K. Mogi, *Bull. Earthquake Res. Inst.* **36**, 99 (1958).
16. If we assume a radius of 200 (± 92) m for the spherical source, the pressure change is on the order of 0.1 (± 1.0) MPa for typical large eruptions, which amounts to about 0.5 (± 5.0)% of the lithostatic pressure (20 MPa).
17. Y. Tanaka, *J. Volcanol. Geotherm. Res.* **2**, 319 (1993).
18. K. Wohletz and G. Heiken, *Volcanology and Geothermal Energy* (Univ. of California Press, Berkeley, 1992).
19. S. W. Kiefer and B. Sturtevant, *J. Geophys. Res.* **89**, 8523 (1984).
20. S. W. Kiefer, *ibid.* **82**, 2895 (1977).
21. The durations of the small eruptions at Aso volcano may be interpreted by the "choked flow" model of the conduit flow of fluid-rock mixture (*19*). Suppose that the conduit pressure is lithostatic at a depth near 1000 m (~20 MPa), where fluid-rock mixture starts ascending (*18*), and the mixture behaves as ideal gas. After 10 to 20 s of initial fluid-rock mixture flow to the bottom of cap rocks below the crater, there would be a good connection of fluid-rock mixture from the starting depth to the cap rocks, building up an excess pressure on the order of 10 MPa below the cap rocks (*18, 23*). When the cap rocks finally fracture, the explosive discharge of a large volume of fluid-rock mixture into the atmosphere occurs. The flow would quickly reach a nearly steady state and be choked at the vent of the conduit with a velocity of sound. This flow may be approximated as a one-dimensional steady flow out of a tank (which is the conduit in this case). The choked flow will be sustained until the pressure at the orifice decreases to the atmospheric value (0.1 MPa) (*19*), corresponding to the tank pressure P_f about 0.18 MPa (for a γ, isentropic exponent, of 1.4). The duration of choked flow is described as $Vt(\gamma,P_0/P_f)/Ac_0$, where V, A, and c_0 are, respectively, tank volume, area of the orifice, and the initial sound velocity in the tank. The constant $t(\gamma,P_0/P_f)$ depends on γ and P_0/P_f, where P_0/P_f is the ratio of initial and final tank pressures, and takes a value near 4.5 for $P_0/P_f = 50$ (*19*). As the fluid-rock mixture is expected to have $c_0 \approx 100$ m/s in the conduit and V/A may be approximated with the length of the conduit, 1000 m, the duration of the flow would be 40 to 50 s, which is close to the observed values. The temperature below the crater at Aso is poorly known, but the above scenario would be rather insensitive to the details of temperature profiles.
22. The large SPT amplitudes and long duration for the large eruptions can be qualitatively interpreted in the framework of the choked flow model. If fluid-rock mixtures flow not only from the conduit but also out of the reservoir itself, the volume-orifice ratio (V/A) should be effectively larger, and the duration is correspondingly longer. When the fluid-rock mixture deeper in the reservoir is tapped, it naturally gains a larger excess pressure at the bottom of the cap rocks, resulting in a larger mass flow rate, which changes as AP_0/c_0 (*19*), corresponding to a larger SPT amplitude.
23. T. Gold and S. Soter, *Pure Appl. Geophys.* **122**, 492 (1985).

24. We thank Aso meteorological station for allowing us to deploy our instruments at its observation sites and for providing various data on the surface activity of Aso volcano. B. Chouet provided helpful comments on an earlier version of the manuscript. R. J. Geller critically reviewed the manuscript.

27 November 1995; accepted 10 June 1996

Impairment of Hippocampal Mossy Fiber LTD in Mice Lacking mGluR2

Mineto Yokoi, Katsunori Kobayashi, Toshiya Manabe, Tomoyuki Takahashi, Isako Sakaguchi, Goro Katsuura, Ryuichi Shigemoto, Hitoshi Ohishi, Sakashi Nomura, Kenji Nakamura, Kazuki Nakao, Motoya Katsuki, Shigetada Nakanishi*

Subtype 2 of the metabotropic glutamate receptor (mGluR2) is expressed in the presynaptic elements of hippocampal mossy fiber–CA3 synapses. Knockout mice deficient in mGluR2 showed no histological changes and no alterations in basal synaptic transmission, paired-pulse facilitation, or tetanus-induced long-term potentiation (LTP) at the mossy fiber–CA3 synapses. Long-term depression (LTD) induced by low-frequency stimulation, however, was almost fully abolished. The mutant mice performed normally in water maze learning tasks. Thus, the presynaptic mGluR2 is essential for inducing LTD at the mossy fiber–CA3 synapses, but this hippocampal LTD does not seem to be required for spatial learning.

Long-lasting modifications in synaptic efficacy at the mossy fiber–CA3 synapses in the hippocampus result from changes in presynaptic cells (*1–4*). In situ hybridization analysis and mGluR2 immunostaining after dentate gyrus lesion indicated that mGluR2 is predominantly expressed in dentate gyrus granule cells (*5*) and selectively distributed to mossy fibers (*6*). By contrast, mGluR2 is absent from the Schaffer collateral-commissural fiber–CA1 synapses (*5, 6*). Furthermore, immunoelectron micros-

copy indicated a unique localization of mGluR2 at the preterminal zone of mossy fibers (Fig. 1).

We investigated the role of the presynaptic mGluR2 in synaptic plasticity in the mossy fiber–CA3 synapses by targeted disruption of the gene encoding mGluR2 (*7*). Southern (DNA), Northern (RNA), and protein immunoblot analyses confirmed the lack of mGluR2 expression. The mGluR2-deficient mice showed no behavioral abnormalities nor any gross anatomical changes in the brain. Synaptic contacts between mossy fiber terminals and spines of the pyramidal neurons of CA3 were no different in wild-type and mutant mice. Intense immunoreactivity for mGluR2 was observed within the stratum lucidum of CA3 and the stratum lacunosum-moleculare of CA1 in the wild-type hippocampus. This immunostaining was not seen in mutant mice, and only weak immunoreactivity, due to cross-reactivity with mGluR3 (*8*), was detected at the molecular layer of the dentate gyrus (Fig. 2, A and B).

We investigated electrophysiological responses at the mossy fiber–CA3 synapses in slice preparations with standard extracellular recording techniques (*3*, *4*). Although there was some slight variation in the time course of the field excitatory postsynaptic potential (EPSP) evoked by stimulation of mossy fibers, no consistent difference in the amplitude of EPSPs relative to that of the fiber volley was detected between wild-type (213 ± 24%) and mutant mice (229 ± 27%) (mean ± SEM; n = 25 each; $P > 0.6$) (*9*). Paired-pulse facilitation (50-ms interpulse interval) (*2*, *10*) was no different in wild-type (n = 7, 214 ± 10%) and mutant mice (n = 8, 229 ± 15%) (mean ± SEM, $P > 0.4$).

Exogenous activation of presynaptic mGluRs inhibits synaptic responses at the mossy fiber–CA3 synapses (*11*). Because (2*S*,1′*R*,2′*R*,3′*R*)-2-(2,3-dicarboxycyclopropyl)glycine (DCG-IV) acts as a potent and selective agonist for mGluR2 or mGluR3 (*12*), we tested the effect of DCG-IV on synaptic responses at the mossy fiber synapses. Bath application of DCG-IV markedly and reversibly depressed EPSPs in wild-type mice, but this depression was greatly reduced in mutant mice (Fig. 3A). Although the observed reduction was partial, probably due to the presence of another DCG-IV–sensitive mGluR3 (*6*), these results indicate that presynaptic mGluR2 contributes a large fraction of the presynaptic inhibition at the mossy fiber–CA3 synapse.

Mossy fiber–CA3 synapses exhibit *N*-methyl-D-aspartate (NMDA) receptor–independent LTP after tetanic stimulation (*13*), and this LTP is presynaptic (*2*, *3*). Prolonged low-frequency stimulation (LFS) induces homosynaptic LTD at these synapses in hippocampal slices (*4*). This LTD also occurs by a presynaptic mechanism that is independent of postsynaptic cell depolarization and NMDA receptors (*4*). LTP at the mossy fiber–CA3 synapses was induced normally in mGluR2-deficient mice after tetanic stimulation (100 Hz, 1 s) (Fig. 3B); the amplitudes of EPSPs 60 min after tetanus were 152.5 ± 7.1% for wild-type mice (n = 6) and 161.7 ± 10.6% for mutant mice (n = 6) (mean ± SEM, $P > 0.4$). Furthermore, slightly suprathreshold tetanic stimulation (100 Hz, 200 ms) induced similar extents of LTP between wild-type (126.8 ± 4.5%) and mutant mice (117.9 ± 7.3%) (n = 5 each, $P > 0.3$). In contrast, LTD at the mossy fiber–CA3 synapses was significantly impaired in mutant mice (Fig. 3, C and D). In wild-type mice, EPSPs were facilitated during LFS and then decreased below control levels after LFS. This depression lasted for at least 45 min. In mutant mice, the facilitation of EPSPs and the subsequent short-term depression (STD) were unchanged. However, this depression was transient and EPSPs returned gradually to control levels; the amplitudes of EPSPs 45 min after LFS were 78.8 ± 3.9% for wild-type mice (n = 10) and 95.0 ± 2.7% for mutant mice (n = 11) ($P < 0.002$).

LTD in the CA1 region of the hippocampus has been implicated in the underlying mechanism of spatial learning (*14*). To test for the involvement of mossy fiber LTD in spatial learning, we performed the Morris water maze tasks (*15*, *16*). The wild-type and mutant mice showed no differences in their ability to perform either the visible- or hidden-platform tasks (Fig. 4, A and B). In a transfer test, the wild-type and mutant mice exhibited no differences in either the time spent or the number of crossings in the trained quadrant (Fig. 4, C and D).

We also examined the ability of trained mice to adapt to a new platform with a 4-day retraining regimen (*16*). Although spatial response reversal is thought to correlate with the function of the basal ganglia (*17*), this test also permits the evaluation of spatial learning flexibility. In the reversal test, the wild-type and mutant mice (n = 12 each) showed no differences in latencies to find the new platform location ($P > 0.14$), the time spent ($P > 0.67$), and the number of crossings ($P > 0.82$) in the newly trained quadrant. These observations demonstrate that impairment of mossy fiber LTD due to mGluR2 deficiency does not hinder spatial learning in a water maze.

The extent of inhibition of mossy fiber LTD by a competitive mGluR antagonist (*4*) was comparable to that observed in mGluR2-deficient mice, which indicates that mGluR2 serves as a predominant and selective receptor for induction of mossy fiber LTD. Accumulating glutamate during LFS may thus activate the presynaptic mGluR2 and induce LTD at the mossy fiber synapses. Furthermore, mGluR2, when expressed in CHO cells, is coupled to inhibition of the adenosine 3,5′-monophosphate (cAMP) cascade (*18*). Stimulation of the cAMP cascade underlies the induction of LTP at the mossy fiber–CA3 synapses (*1*);

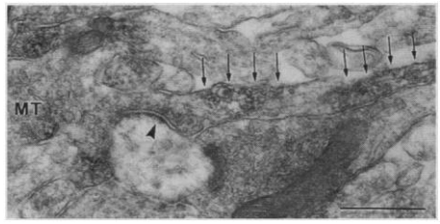

Fig. 1. Immunoelectron microscopy of mouse mossy fiber–CA3 synapses. mGluR2 immunoreactivity (arrows) is seen at the preterminal zone rather than at the synaptic junction (arrowhead) of mossy fibers; MT, a mossy fiber terminal. Immunoelectron microscopy was carried out as described (*8*). Scale bar, 0.5 μm.

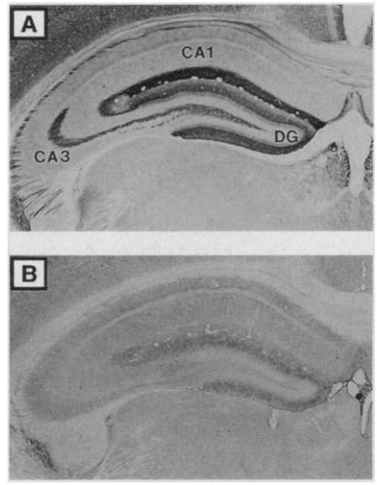

Fig. 2. Immunocytochemical analyses of the hippocampus. Hippocampal coronal sections of littermates (14 weeks old) of wild-type (**A**) and mutant (**B**) mice were subjected to immunostaining with the mGluR2 antibody; DG, dentate gyrus.

M. Yokoi and S. Nakanishi, Department of Biological Sciences (formerly Institute for Immunology), Kyoto University Faculty of Medicine, Kyoto 606, Japan.
K. Kobayashi, T. Manabe, T. Takahashi, Department of Neurophysiology, Institute for Brain Research, Faculty of Medicine, University of Tokyo, Tokyo 113, Japan.
I. Sakaguchi and G. Katsuura, Aburahi Laboratories, Shionogi and Company, Ltd., Shiga 520-34, Japan.
R. Shigemoto and H. Ohishi, Department of Morphological Brain Science, Kyoto University Faculty of Medicine, Kyoto 606, Japan.
S. Nomura, College of Medical Technology, Kyoto University, Kyoto 606, Japan.
K. Nakamura, K. Nakao, M. Katsuki, Medical Institute of Bioregulation, Kyushu University, Fukuoka 812, Japan.
*To whom correspondence should be addressed.

Ca^{2+} entry into the presynaptic terminal activates Ca^{2+}-calmodulin–sensitive adenylyl cyclase 1, which would, in turn, produce LTP through protein kinase A. Bidirectional modification of synaptic efficacy, such as LTP and LTD, may thus occur by regulation of the cAMP cascade at the presynaptic site of the mossy fiber–CA3 synapses.

In mGluR2-deficient mice, STD normally occurs at the mossy fiber–CA3 synapses after LFS. Thus, the direct involvement of STD in spatial learning cannot be excluded. Notably, ablation of protein kinase A by gene targeting produces a selective defect in mossy fiber LTP (*19*), and the elimination of mossy fiber LTP does not affect spatial learning (*19*). Thus, contrary to current theories about hippocampal function, neither LTP nor LTD at the mossy fiber–CA3 synapses appears to be required for spatial learning, although they may have a variety of other physiological roles.

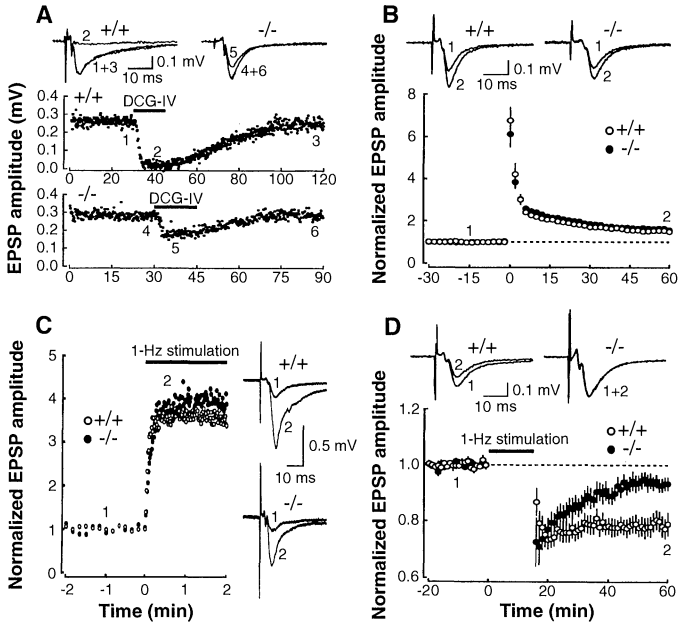

Fig. 3. Inhibition of excitatory synaptic transmission by DCG-IV and LTP and LTD at mossy fiber–CA3 synapses. Representative data of the DCG-IV effect on CA3 synaptic responses of wild-type (+/+) and mutant (−/−) mice are indicated (**A**); the extents of the synaptic inhibition with 1.0 μM DCG-IV were 94.1 ± 2.1% for wild-type mice (n = 4) and 44.8 ± 9.9% for mutant mice (n = 3) (mean ± SD, P < 0.0002); at 0.1 μM DCG-IV (*20*), inhibition was 52.7 ± 8.4% for wild-type mice (n = 7) and 17.0 ± 4.1% for mutant mice (n = 7) (mean ± SD, P < 0.0001). A similar DCG-IV effect was observed in the presence of 25 μM D-(−)-2-amino-5-phosphonovalerate (D-AP5), an NMDA receptor antagonist. LTP induced by tetanic stimulation (100 Hz, 1 s) given once (**B**) and the facilitation (**C**) and the subsequent LTD (**D**) elicited by LFS (1 Hz, 15 min) were recorded in slices from wild-type and mutant littermates (8 to 15 weeks old). The facilitation of EPSPs at the beginning and at the end of LFS was not different between wild-type mice (437 ± 29% and 299 ± 17%, n = 9) and mutant mice (428 ± 24% and 294 ± 18%, n = 8) (P > 0.8). Traces represent sample EPSPs recorded at the times indicated by the numbers on the corresponding graphs; in (D), EPSPs returned to control levels 45 min after LFS in 8 of 11 slices of mutant mice, as indicated in the sample trace. Mossy fiber EPSPs were recorded as described (*4*); mossy fibers were stimulated at 0.1 Hz; D-AP5 (25 μM) was applied before tetanic stimulation; D-AP5 (25 μM) was confirmed to have no effect on LTD (*4*). All experiments examining LTP and LTD were performed in a blinded fashion.

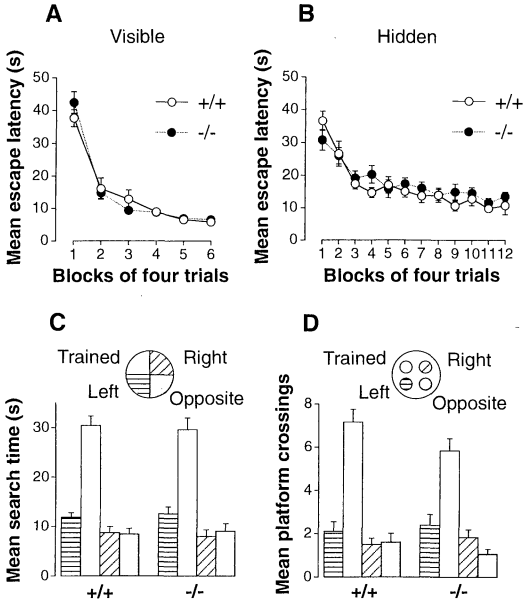

Fig. 4. Morris water maze test of wild-type and mutant mice. In both a visible-platform task (**A**) and a hidden-platform task (**B**), the performances of wild-type (+/+) and mutant (−/−) mice (n = 18 each) improved during training [visible, $F(5,170)$ = 107.057, P < 0.0001; hidden, $F(11,374)$ = 21.628, P < 0.0001], and there was no difference between the two genotypes [visible, $F(1, 34)$ = 0.008, P = 0.9297; hidden, $F(1, 34)$ = 0.615, P = 0.4383]. In the transfer test, no significant difference was noted in the time spent (P > 0.78) (**C**) and the number of crossings (P > 0.11) (**D**) in the trained quadrant. The animals used were 8 to 23 weeks old. Bars indicate the SEM.

REFERENCES AND NOTES

1. M. G. Weisskopf, P. E. Castillo, R. A. Zalutsky, R. A. Nicoll, *Science* **265**, 1878 (1994); Y.-Y. Huang, X.-C. Li, E. R. Kandel, *Cell* **79**, 69 (1994); R. A. Nicoll and R. C. Malenka, *Nature* **377**, 115 (1995).
2. R. A. Zalutsky and R. A. Nicoll, *Science* **248**, 1619 (1990).
3. P. E. Castillo, M. G. Weisskopf, R. A. Nicoll, *Neuron* **12**, 261 (1994).
4. K. Kobayashi, T. Manabe, T. Takahashi, *Science* **273**, 648 (1996).
5. H. Ohishi, R. Shigemoto, S. Nakanishi, N. Mizuno, *Neuroscience* **53**, 1009 (1993).
6. R. Shigemoto *et al.*, *Int. Brain Res. Org. Abstr.* **4**, A3.41 (1995); R. Shigemoto *et al.*, *Soc. Neurosci. Abstr.* **21**, 338.20 (1995).
7. We generated mGluR2-deficient mice as described [M. Masu *et al.*, *Cell* **80**, 757 (1995)]. The 15.3-kb DNA fragment containing exon 2 of the gene encoding mGluR2 was isolated from a 129/Sv mouse genomic library. For gene targeting, the translation initiation site and its downstream sequence in exon 2 were disrupted by replacement of this exon with the neomycin resistance gene. Germ-line transmission was achieved with two independent embryonic stem cell lines containing the properly targeted mGluR2 gene. Littermates of the F_2 or F_3 generation of wild-type and mutant mice were used for all experiments.
8. H. Ohishi *et al.*, *Neuron* **13**, 55 (1994).
9. EPSPs ranging from 0.15 to 0.25 mV were recorded from 25 slice preparations, and the relative amplitudes of EPSP–fiber volley were determined.
10. T. Manabe, D. J. A. Wyllie, D. J. Perkel, R. A. Nicoll, *J. Neurophysiol.* **70**, 1451 (1993).
11. T. H. Lanthorn, A. H. Ganong, C. W. Cotman, *Brain Res.* **290**, 174 (1984); O. J. Manzoni, P. E. Castillo, R. A. Nicoll, *Neuropharmacology* **34**, 965 (1995).
12. Y. Hayashi *et al.*, *Nature* **366**, 687 (1993).
13. E. W. Harris and C. W. Cotman, *Neurosci. Lett.* **70**, 132 (1986).
14. A. Abeliovich *et al.*, *Cell* **75**, 1263 (1993); M. Mayford, J. Wang, E. R. Kandel, T. J. O'Dell, *ibid.* **81**, 891 (1995); M. E. Bach, R. D. Hawkins, M. Osman, E. R. Kandel, M. Mayford, *ibid.*, p. 905.
15. R. G. M. Morris, *Learn. Motiv.* **12**, 239 (1981).
16. Animals were allowed 60 s to locate the platform (6 cm in diameter), which was submerged by 0.5 cm in a water pool (90 cm in diameter). Once the animal found the platform, it was allowed to remain there for 30 s. Animals were put through 12 trials per day in three sessions of four trials each. The visible-platform task was carried out on days 1 and 2. From days 13 to 16, the mice were trained in the hidden-platform task. On day 17, we performed the transfer test by allowing mice to swim for 60 s in the pool after the platform had been removed. For the reversal trial, the platform was moved to the opposite quadrant, and the mice were retrained from days 18 to 21. On day 22, the platform was again removed from the pool, and the transfer test was carried out.
17. R. J. McDonald and N. M. White, *Behav. Neural Biol.* **61**, 260 (1994); J. Nasir *et al.*, *Cell* **81**, 811 (1995).
18. Y. Tanabe, M. Masu, T. Ishii, R. Shigemoto, S. Nakanishi, *Neuron* **8**, 169 (1992).
19. Y.-Y. Huang *et al.*, *Cell* **83**, 1211 (1995).
20. M. Yokoi *et al.*, data not shown.

21. We thank A. Uesugi for photographic assistance. This work was supported by grants from the Ministry of Education, Science, and Culture in Japan.

20 February 1996; accepted 4 June 1996